Available online at www.sciencedirect.com
ScienceDirect
Trans. Nonferrous Met. Soc. China 26(2016) 2976−2987
Transactions of Nonferrous Metals Society of China
www.tnmsc.cn

Electrodeposition and corrosion resistance of Ni−P−TiN composite coating on AZ91D magnesium alloy

Ya-ru ZHOU[1], Shan ZHANG[1], Lin-lin NIE[1], Ze-jie ZHU[1], Jian-qing ZHANG[1], Fa-he CAO[1], Jun-xi ZHANG[2]

1. Department of Chemistry, Zhejiang University, Hangzhou 310027, China;
2. Shanghai Key Laboratory of Materials Protection and Advanced Materials in Electric Power, Shanghai University of Electric Power, Shanghai 200090, China

Received 8 October 2015; accepted 9 May 2016

Abstract: In order to improve the corrosion resistance and microhardness of AZ91D magnesium alloy, TiN nanoparticles were added to fabricate Ni−P−TiN composite coating by electrodeposition. The surface, cross-section morphology and composition were examined using SEM, EDS and XRD, and the corrosion resistance was checked by electrochemical technology. The results indicate that TiN nanoparticles were doped successfully in the Ni−P matrix after a series of complex pretreatments including activation, zinc immersion and pre-electroplating, which enhances the stability of magnesium alloy in electrolyte and the adhesion between magnesium alloy and composite coating. The microhardness of the Ni−P coating increases dramatically by adding TiN nanoparticles and subsequent heat treatment. The corrosion experimental results indicate that the corrosion resistance of Ni−P−TiN composite coating is much higher than that of uncoated AZ91D magnesium alloy and similar with Ni−P coating in short immersion time. However, TiN nanoparticles play a significant role in long-term corrosion resistance of composite coatings.
Key words: AZ91D; composite coating; TiN nanoparticle; electrodeposition; corrosion resistance

1 Introduction

Magnesium and its alloy have been used in many industrial applications such as telecommunications, aerospace, automotive, microelectronics and recreational equipment as they possess excellent properties [1,2]. However, poor corrosion and wear resistance, high chemical and electrochemical reactivity of magnesium and its alloy hinder their widespread use in many applications [3,4]. Therefore, numerous surface modification methods such as electro/electroless plating, physical−chemical vapor depositions, conversion coatings, and thermal spray coating were presented for producing corrosion-resistant coatings on magnesium alloy [5−7].

Since electrodeposition provides the alloy substrate with coatings showing excellent corrosion and wear resistance properties and convenience of operation, it is considered a relatively effective choice among various surface coatings treatments [8,9]. It was reported that electrodeposition of Ni−P alloy coatings enhances the corrosion resistance, microhardness and wear resistance of magnesium [5,6]. Ni−P−X composite coatings with better corrosion properties and higher hardness have already been deposited on magnesium alloy by adding ceramic powders such as TiO_2 [10], SiC [11], Si_3N_4 [12], BC [13] and Al_2O_3 [14] reinforcing particles using either electroless or electroplating techniques. YANG et al [15] have developed a novel electroless deposition to produce nanoparticle ZrO_2 reinforced metal coatings on AZ31 magnesium alloy. LIU et al [16] found that abrasive wear was dominant for Ni−P−WC composite coating due to the existence of embedded WC nanoparticles. Since the nanoparticles are dispersed in the matrix, the content and nature of particles in the coatings dominate the corrosion and wear resistance properties of the coating. In another study, it was mentioned that TiN nanoparticles not only have high strength, modulus and hardness but also possess high chemical and thermal stabilities [17,18]. Therefore, it can be presumed that TiN nanoparticle could be used as

Foundation item: Projects (51171172, 51131005) supported by the National Natural Science Foundation of China; Project (R16E010001) supported by Zhejiang Provincial Natural Science Foundation of China; Project (2015QNA3011) supported by Fundamental Research Funds for the Central Universities, China; Project (14DZ2261000) supported by Science and Technology Commission of Shanghai Municipality, China
Corresponding author: Fa-he CAO; Tel: +86-571-87952318; +86-13588061502; E-mail: nelson_cao@zju.edu.cn
DOI: 10.1016/S1003-6326(16)64428-X

secondary phase to enhance the strength and toughness of metal or ceramics substrate.

Magnesium alloys react vigorously with atmospheric oxygen and water due to high chemical and electrochemical reactivity [19,20]. Thus, the naturally formed hydroxide and/or oxide films should be removed prior to electrodeposition as these deteriorate the adhesion of an electrodeposited layer. The intermediate layer between substrate and coating not only reduces the potential difference between magnesium and Ni−P−TiN composite coating, but also decreases the corrosion of magnesium during the Ni−P−TiN electroplating process [21]. Therefore, ultrasonic cleaning, acid pickling-activation, and zinc immersion are performed prior to electroplating magnesium [22]. The HF acid pickling-activation step should be done before zinc immersion, which helps to remove the loose oxide/ hydroxide film on the magnesium alloy surface, and then avoids fierce corrosion [23]. Apart from HF, ammonium fluoride was present in the plating to form MgF_2. The chemical activity and Volta potential diversity distribution on the substrate are equalized after zinc immersion process [22,24]. In our previous work [25], semi-bright nickel was electroplated on AZ91D magnesium alloy from an acidic bath as the protective layer for the further electroplating, and then Ni−P coating was directly electroplated on the protective layer.

In the current study, Ni−P−TiN composite coatings were successfully electrodeposited on AZ91D magnesium alloy after some special pretreatments. Since many researchers [26,27] and our group [25] have studied the influence of plating parameters, such as bath temperature, and the content of H_3PO_3 in electrolyte on Ni−P coatings, and the effects of bath pH and current density on the TiN nanoparticle content in the composite coating were studied herein. Furthermore, the effects of incorporation of TiN nanoparticles in Ni−P electro-deposition on microhardness and long-term corrosion resistance of the coatings were also investigated.

2 Experimental

2.1 Preparation of Ni−P−TiN composite coating

The substrate was made of cast AZ91D magnesium alloy. Cylindrical rods (*d*8 mm × 6 mm) sealed with polytetrafluoroethylene (PTFE) and surface area of 0.50 cm^2 were used. The substrate was polished using silicon carbide emery papers of 400 to 1000 grade followed by alumina paste of 2.5 μm. Thereafter, the substrate was degreased in acetone using ultrasonic cleaning device and washed twice using distilled water.

With the purpose of increasing the corrosion resistance and adhesive bond between the coatings and the substrate, some appropriate surface pretreatments were adopted before the composite coatings electro-deposition on AZ91D magnesium alloy [28]. The process flow and main parameters of pre-treatment are shown in Table 1. All solutions were prepared using analytical reagents and deionized water. During experiments, bath temperature was maintained at the required value using thermostatic water bath.

Table 1 Pre-treatment parameters used for electrodeposition of protective coatings on AZ91D magnesium alloy (RT=room temperature)

Process operation	Solution composition	Concentration	Conditions
Degreasing	Acetone	−	RT, 1−3 min
Picking-activation	HF (40%)	54 mL/L	RT, 30 s
Zincate pretreatment	$ZnSO_4·7H_2O$	30 g/L	3.5−5 min, 70 °C pH=10.0±0.2
	$K_4P_2O_7$	180 g/L	
	Na_2CO_3	5 g/L	
Cu electrodeposition (undercoatings)	$Cu_2P_2O_7$	28 g/L	12 min, 40 °C
	$K_4P_2O_7$	100−150 g/L	pH=8.2−8.8
	$(NH_4)_3C_6H_5O_7$	60−70 g/L	D_k=1.20 A/dm^2
Ni electrodepositon	$NiSO_4·6H_2O$	240 g/L	10 min, 45 °C pH=5.5−6.0 D_k=4.0 A/dm^2
	$NiCl_2·6H_2O$	45 g/L	
	H_3BO_3	40 g/L	
	NH_4F	20 g/L	

Before electrodeposition, TiN nanoparticles and the surfactant were added to plating bath using ultrasonic dispersion for 12 h to ensure a good dispersion of TiN nanoparticles [29]. TiN nanoparticles obtained from Hefei Kaier Nanometer Energy & Technology, China, have an average particle size of approximately 20 nm. During the plating process, the electrolyte was agitated by mechanical impeller to maintain the uniform particulate concentration and prevent sedimentation of the TiN nanoparticles. Main parameters for electro-deposition of Ni−P−TiN composite coatings on AZ91D magnesium alloy are presented in Table 2. The fabrication technique of Ni−P alloy coating was given in our previous work [25].

2.2 Microstructure characterization and electro-chemical measurement

The surface morphologies of coatings were investigated using SU8010 (Hitachi, Japan) and SIRION (FEI Co., Holland) scanning electron microscope (SEM) operated at 25 kV. The chemical composition of the composite coatings were analyzed using energy dispersive spectroscopy (EDS) equipped with SEM. The microstructure of coating was characterized using a transmission electron microscope (TEM, JEOL20OCX, Japan). The crystal structure was determined using X-ray

diffraction (XRD, XPERT-PRO, PANalytical B.V., Holland) with a Cu K_α radiation in the 2θ range of 20°−80° with an operating target voltage of 50 kV and a tube current of 100 mA using a scan step of 0.04°.

Table 2 Parameters for electrodeposition of Ni−P−TiN coatings on AZ91D magnesium alloy

Plating bath composition	Concentration/ ($g \cdot L^{-1}$)	Parameter	Value
$NiSO_4 \cdot 6H_2O$	200	Current density/($A \cdot dm^{-2}$)	4.0, 5.0, 6.0, 8.0
$NiCl_2 \cdot 6H_2O$	45	Plating time/ min	30, 24, 20, 15
H_3PO_3	40	Bath pH	1.5−3.0
H_3PO_4	30	Bath temperature/°C	70±5
TiN	5	Agitation speed/($r \cdot min^{-1}$)	600
SDS	0.1		

A transistor constant potential/current device (Model ZF−9, China) was used as direct current power source in electroplating process. The conventional three-electrode flat cell was chosen to measure the electrochemical properties in 3.5% NaCl solution at room temperature ((25±0.5) °C) [30]. A saturated calomel electrode (SCE) and a large platinum sheet were used as reference electrode and auxiliary electrode, respectively. The film was coated on the AZ91 magnesium alloy with exposed area of 0.5 cm^2 as working electrode.

After obtaining a relatively stable open circuit potential (OCP), potentiodynamic polarization was performed using CHI630C electrochemical workstation (Shanghai Chenhua Instruments Company, China). Electrochemical impedance spectroscopy (EIS) was performed using a VMP2 multichannel potentiostat (PARC, USA). The Tafel curves were recorded at a scanning rate of 0.5 V/s from −0.2 to 1 V versus OCP in neutral NaCl solutions in order to evaluate the anticorrosion performance of Ni−P−TiN composite coatings. Current response was recorded and analyzed by extrapolating the Tafel curve. The EIS measurements were conducted at the OCP and acquired in the frequency range of 100 kHz to 0.01 Hz using a 10 mV amplitude sine wave generated by a frequency response analyzer. The potentials were reported with respect to SCE in the current work.

3 Results and discussion

3.1 Effect of electroplating parameter on Ni−P−TiN composite coating

3.1.1 Electroplating current density (D_k)

The influence of current density was studied when other electroplating parameters remained constant. The constant parameters are: TiN concentration 5 g/L, pH 1.5, solution agitation speed 600 r/min, and bath temperature (70±5) °C. The influence of D_k on the Ti and P element contents of Ni−P−TiN composite coatings is presented in Fig. 1. It is evident that with increasing the current density from 3.0 to 8.0 A/dm^2, Ti content in the composite coatings increases initially and decreases afterwards, while P content reduces (Fig. 1). The Ti content peaked at 6.0 A/dm^2. In addition, it is clear that doping nanoparticles have less effect on the P content in the coatings. The P content in Ni−P−TiN composite coatings is found to be slightly lower than that in Ni−P alloy coatings under the same current density [25], which is mainly attributed to the deposition mechanism and correspondent with the change of P content in Ni−P alloy electroplating [31]. However, electroplating current density has a significant influence on the TiN content of the composite coatings. The electric field force of plating bath and the electrostatic repulsive force between cathode surface and negatively charged TiN particle [32] increase with increasing current density. This causes low transport rate of nanoparticles to the cathode and TiN content in the coating [33]. Finally, D_k was chosen as 6.0 A/dm^2 for subsequent experiment.

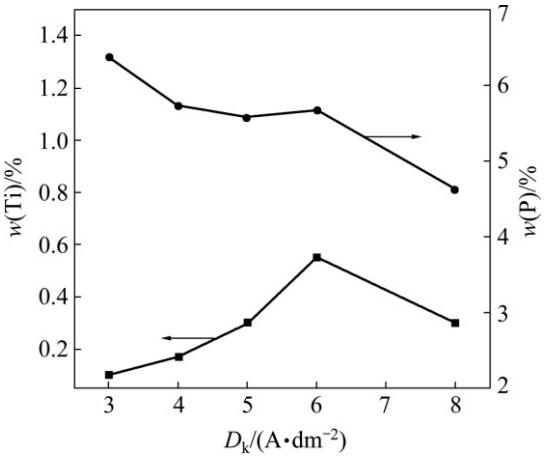

Fig. 1 Influence of D_k on Ti and P contents of Ni−P−TiN coatings (Temperature 70 °C, pH 1.5, solution agitation speed 600 r/min)

3.1.2 Bath pH

The influence of bath pH was studied when the other electroplating parameters remained fixed, which are TiN concentration 5 g/L, D_k 6.0 A/dm^2, solution agitation speed 600 r/min and bath temperature 70 °C. Figure 2 shows Ti content of Ni−P−TiN composite coatings with respect to plating solution pH. It is obvious that Ti content in composite coating increases initially and decreases afterwards with increasing pH value from pH 1.5 to 3.0 (Fig. 2). It is worth mentioning that Ti

content peaked at pH 2.0. The effect of plating bath pH on the nanoparticle TiN content can be attributed to the fact that different pH values might result in the change of surface charge on substrate and nanoparticle [34,35]. As a result, the TiN nanoparticle content of the composite coating appears to be higher at pH 2.0 than that at pH 3.0. So, it can be reported that TiN content increases with increasing pH up to a certain value. Beyond this value/point, the TiN nanoparticle content decreases. The lower H^+ concentration at higher pH reduces the volume of nanoparticles adsorbed by H^+ ions, thus TiN content in the coatings reduces [26].

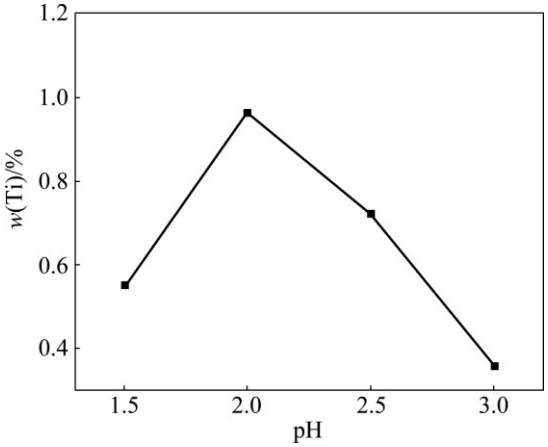

Fig. 2 Influence of bath pH on Ti content of Ni−P−TiN composite coatings (Temperature 70 °C, D_k=6.0 A/dm^2, solution agitation speed 600 r/min)

In conclusion, TiN content in the composite coatings would be optimum under the electroplating conditions of pH 2.0, D_k 6.0 A/dm^2, TiN concentration 5 g/L, bath temperature 70 °C and agitation speed 600 r/min.

3.2 Characterization of Ni−P−TiN composite coatings

3.2.1 Surface morphology and microstructure

Figure 3(a) shows the microstructure of TiN nanoparticles. The average size of sphere-shaped TiN nanoparticle is found to be around 20 nm. Figure 3(b) shows the XRD pattern for TiN nanoparticles. The diffraction peaks of (111), (200), (220), (311) and (222) planes are the characteristics of TiN nanoparticles.

The typical surface morphology and microstructure of Ni−P coating with different magnifications are shown in Figs. 4(a) and (b), while those of Ni−P−TiN composite coatings are shown in Figs. 4(c) and (d). It is obvious that the morphology of the coating changes after TiN nanoparticles addition. It can be seen that TiN nanoparticles have embedded in the N−P matrix by codeposition. Some of the TiN nanoparticles agglomerate to a certain extent in spite of mechanical/ magnetic agitation used before electrodeposition. As shown in Fig. 4(a), nodular structures are distributed

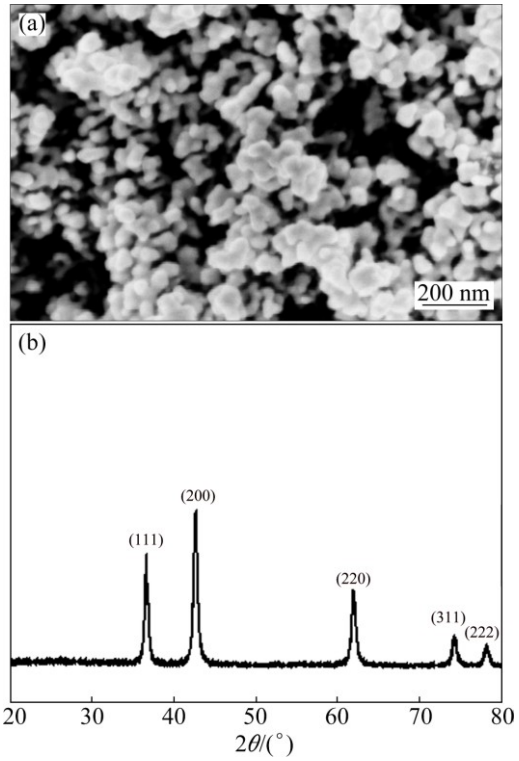

Fig. 3 SEM image (a) and XRD pattern (b) of TiN nanoparticles

uniformly in the Ni−P microstructure, and the size of Ni−P particle shown in Fig. 4(b) is around 50 nm. In the case of Ni−P−TiN specimen, the nodules are found to be much smaller in size and the surface appears to be smooth as shown in Figs. 4(c) and (d). It can be concluded from Figs. 4 (a)–(d), that the TiN nanoparticles can refine the crystal grains. Figure 4(e) shows the bright-field TEM micrograph of Ni−P−TiN composite coatings. It can be found that TiN nanoparticles are embedded into the Ni−P matrix as stripe mosaic and dispersed well. In addition, few of the TiN nanoparticles agglomerated in composite membrane coatings. The selected-area electron diffraction (SAD) pattern of the same sample is shown in Fig. 4(f), where the arrow-pointed (220), (222), (200), and (220) faint diffraction rings correspond to the TiN crystal parameter. Figure 4(g) shows that peak intensity of Ti element energy spectrum is relatively weak, due to the low content of Ti (0.96%). It can be seen that there are some dark TiN nanoparticles pointed by arrow in Fig. 4(e), which are further demonstrated by composite coating TEM diffraction pattern and the energy spectrum of the composite coatings (Figs. 4 (f) and (g)). Based on the above results and analysis, it can be said that although TiN content is not very high, TiN nanoparticles do exist in Ni−P composite coatings.

The cross-section image and corresponding EDS

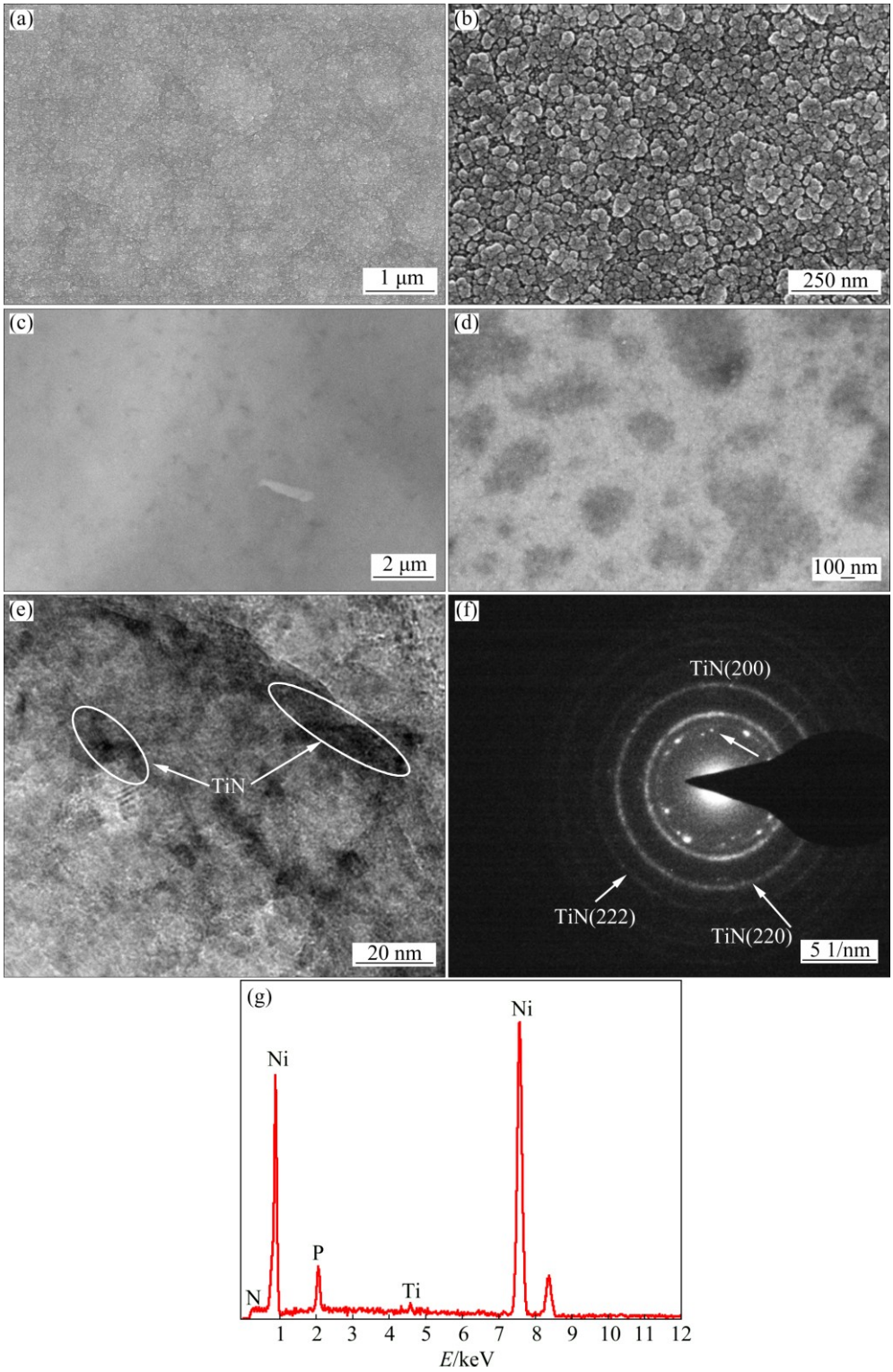

Fig. 4 Typical SEM images of Ni−P coating (a, b) and Ni−P−TiN composite coating (c, d) with different magnifications, TEM bright-field image (e), SAD pattern (f) and EDS analysis of Ni−P−TiN composite coating (g) (Ni−P−TiN composite coating was electrodeposited at pH 1.5, D_k 6 A/dm^2, solution agitation speed 600 r/min and temperature 70 °C)

line profile of the Ni−P−TiN composite coating are shown in Fig. 5. The immersion zinc layer is located in the area where the substrate surface and Cu layer are mutually overlapped, which is similar to our previous work [25]. Though the substrate is not uniformly covered with a coherent Zn layer as shown in Fig. 5(b), the Zn layer strengthens the adhesion of the subsequently deposited Cu layer to AZ91D alloy substrate. There is no obvious boundary or interfacial defects observed along the interface between the Cu, Ni and Ni−P−TiN layers

shown in Fig. 5(a), indicating that Ni−P−TiN composite coating is attached tightly to the Ni layer, which is also attached tightly to the Cu underlayer. In addition, the Ni−P−TiN composite coating is compact and no pores exist in its cross-section morphology. As shown in Fig. 5(b), the corresponding element distribution from the coating surface to the substrate along the line is labeled. Due the low content of TiN nanoparticle in the composite coatings, there are no obvious peaks for Ti and N elements in the EDS line profile, but the P element is very clear. As shown in Fig. 5(b), the thicknesses for Ni−P−TiN, Ni and Cu layers are around 10, 8 and 4 μm respectively, while the Zn layer and AZ91D magnesium alloy substrate are connected tightly.

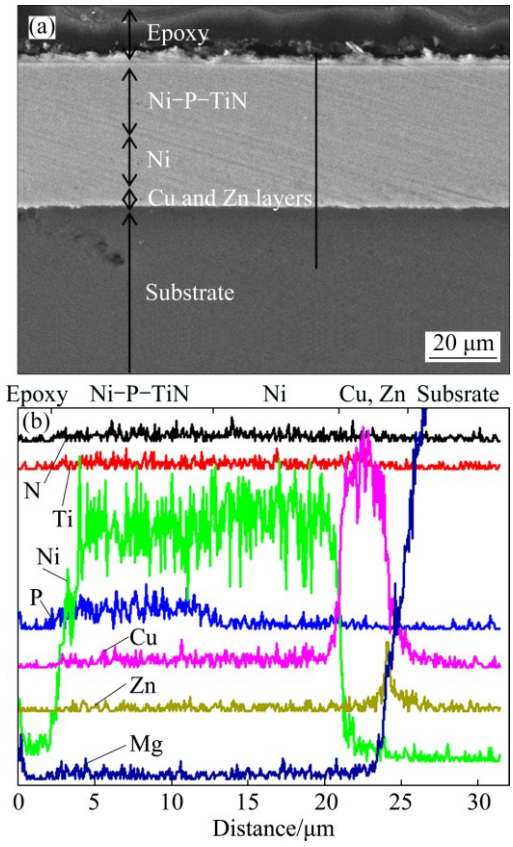

Fig. 5 Cross section morphology (a) and EDS line profile (b) for Ni−P−TiN coating electrodeposited at D_k=8.0 A/dm^2 and pH 2.0

3.2.2 Hardness analysis

Vickers hardnesses of the magnesium alloy substrate, Ni−P alloy coatings and Ni−P−TiN composite coatings before and after heat treatment are presented in Fig. 6. The data shown in Fig. 6 indicate that the hardness of magnesium alloy is very small (HV 62) which does not change noticeably before and after heat treatment (HV 68). The microhardnesses of Ni−P coatings and Ni−P−TiN composite coatings on magnesium alloy are found to be significantly higher than the uncoated AZ91D magnesium alloy. Furthermore, the microhardnesses of as-plated and heat treated Ni−P−TiN coatings are higher than those of the conventional Ni−P coatings respectively. However, after heating at 400 °C for 1 h, the hardness of both Ni−P and Ni−P−TiN specimens improves and reaches HV 653 and HV 855, respectively. Figure 7 presents the XRD patterns of Ni−P alloy and Ni−P−TiN composite coatings before and after heat treatments. The broad diffraction peak at 40°−50° in Ni−P alloy without heat treatment corresponds to Ni amorphous structure (Jade PDF software). After heat treatment, Ni−P alloy and Ni−P−TiN composite coatings are crystallized gradually. XRD pattern of Ni−P−TiN composite coatings shows obvious refinement compared with that of as-plated Ni−P alloy. However, the diffraction peaks of Ni indicate crystallization. Thus, it can be claimed that nanoparticles have the effect of grain refining in Ni−P−TiN composite

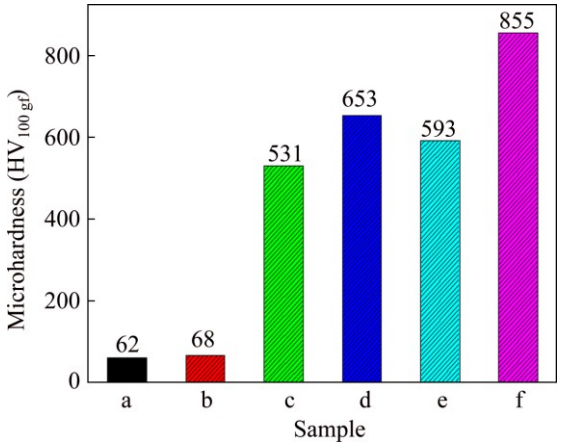

Fig. 6 Microhardness of AZ91D magnesium alloy before (a) and after annealing at 400 °C for 1 h (b), Ni−P coatings before (c) and after annealing at 400 °C for 1 h (d), Ni−P−TiN before (e) and after annealing at 400 °C for 1 h (f) (The electrodepositing parameters are pH 1.5, D_k=6A/dm^2)

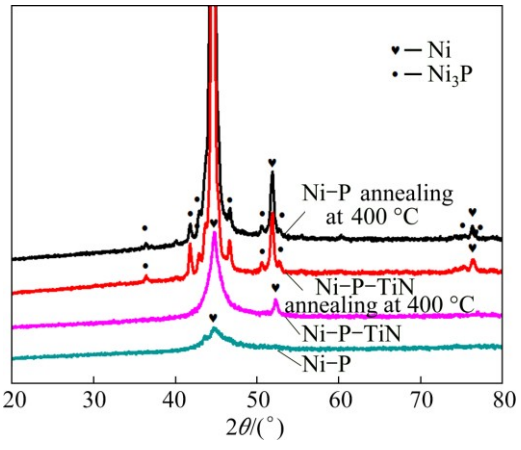

Fig. 7 XRD patterns of Ni−P coatings and Ni−P−TiN composite coatings with and without annealing at 400 °C for 1 h (The electrodepositing parameters are pH 1.5, D_k=6 A/dm^2)

coatings. The hardness of Ni−P−TiN composite coatings is measured to be higher than that of Ni−P alloy. The incorporation of the TiN nanoparticles in the coatings improves the hardness of the specimens due to the high hardness of TiN nanoparticles dispersed in the alloy coatings. It was mentioned that TiN nanoparticles enhance the lattice distortion resistance, improve the density and hardness of the composite coatings without changing organizational structure of Ni−P coating [36,37].

The XRD diffraction peaks from Ni−P alloy and Ni−P−TiN composite coatings become narrow after heat treatment, and new phase, Ni_3P, can also be identified. In addition, the amount of Ni_3P phase in Ni−P−TiN composite coating is found to be more than that in Ni−P alloy, and the Ni_3P phase is in the more disperse state. Due to the high strength of Ni_3P phase, the microhardnesses of both Ni−P with/without TiN increase after heat treatment [38].

In conclusion, the microhardnesses of both kinds of coatings significantly increase due to the presence of Ni−P coating with/without TiN nanoparticle. In addition, heat treatment further improves the microhardness, which can be attributed to the formation of new Ni_3P phase. The Ni−P−TiN composite coating has exhibited significantly improved microhardness compared with the Ni−P coatings after heat treatment.

3.3 Performance of Ni−P−TiN composite coatings

3.3.1 Corrosion resistance

Potentiodynamic polarization curves of AZ91D magnesium alloy, Ni−P coatings and Ni−P−TiN composite coatings immersed in 3.5% NaCl solution for 30 min are shown in the Fig. 8. The Ni−P coatings are fabricated at pH of 2.0, current density of 8 A/dm^2 and without ultrasonic. It can be seen that all the polarization curves of Ni−P−TiN composite coatings and Ni−P coatings show a wider passive region and dramatically smaller corrosion current density than that of uncoated AZ91 magnesium alloy (Fig. 8). This indicates that the electrodeposition of Ni−P−TiN composite coatings and Ni−P coatings improves the corrosion resistance of AZ91D magnesium alloy serving as a protective layer that inhibits corrosion reaction.

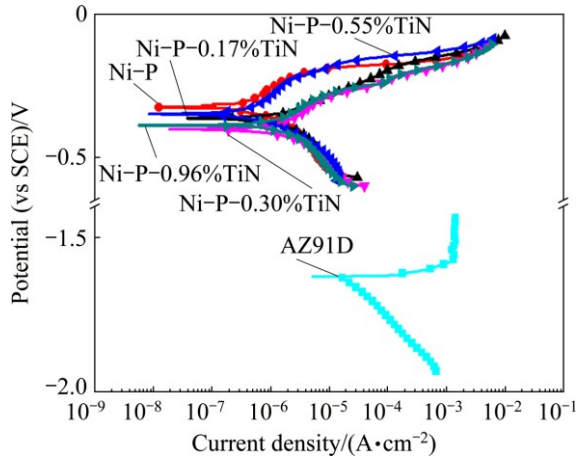

Fig. 8 Polarization curves of substrate, Ni−P coatings and Ni−P−TiN composite coatings in neutral 3.5% NaCl at room temperature (immersion time 30 min, pH 2.0, D_k=8 A/dm^2)

Figure 8 also shows that the TiN content of Ni−P−TiN composite coatings has a slight effect on corrosion potential and corrosion current density. It has been found that the shapes of anode polarization curve of different coatings (Ni−P coatings, Ni−P−0.17%TiN composite coatings and Ni−P−0.30%TiN composite coatings) are identical. The curves corresponding to Ni−P−0.55%TiN and Ni−P−0.96%TiN composite coating show the plateau region on the anodic branch in potential range of 0.23−0.3 V vs SCE. It should be noted that the platform of the latter is not obvious. However, the anodic dissolution principle of Ni−P−TiN composite coatings with low TiN nanoparticles content is consistent with Ni−P alloy coatings but Ni−P−TiN composite coatings with high TiN nanoparticles content show slight passivation phenomena in the process of anodic dissolution.

The electrochemical parameters obtained from polarization curves are presented in Table 3. It shows that the corrosion potential of the AZ91D magnesium alloy is much more negative than the Ni−P coatings and Ni−P−TiN composite coatings. Thus, it can be deduced that the coatings on substrate alloy can extensively improve the corrosion resistance. The data of Table 3 show that Ni−P alloy coating presents better positive corrosion potential, smaller corrosion current density and the best corrosion resistance compared with Ni−P−TiN composite coatings, where both coatings are immersed for 30 min. The corrosion potential and corrosion current density of composite coating with different TiN contents

Table 3 Parameters obtained by fitting polarization curves of specimens

Specimen	φ_{corr}(vs SCE)/V	J_{corr}/ (μA·cm^{-2})	β_c/ (mV·dec^{-1})	β_a/ (mV·dec^{-1})
AZ91D Mg alloy	−1.73	73.15	−196.1	127.71
Ni−P	−0.29	0.54	−175.13	111.56
Ni−P−0.17%TiN	−0.39	1.16	−141.16	102.8
Ni−P−0.30%TiN	−0.38	1.25	−137.9	105.74
Ni−P−0.55%TiN	−0.32	0.62	−141.66	167.7
Ni−P−0.96%TiN	−0.36	1.30	−182.64	98.18

are measured to be in the range of 0.36−0.39 V and 0.62−1.30 μA/cm^2, respectively. The Ni−P−0.55%TiN composite coating presents the smallest corrosion current density (0.62 μA/cm^2) among the studied Ni−P−TiN coatings, which indicates that with increasing the TiN nanoparticle content, the corrosion resistant performance of Ni−P−TiN increases and decreases afterwards. On the other hand, corrosion current density of Ni−P coating is a little bit smaller than that of Ni−P−TiN composite coatings, which indicates that the corrosion resistance of Ni−P coating is slightly higher than its counterpart for 30 min immersion. However, Ni−P−TiN composite coatings immersed in neutral 3.5% NaCl solution have better corrosion resistance properties for a long-term immersion.

3.3.2 Long-term corrosion behavior

Figure 9 shows the OCP of Ni−P−TiN composite coating soaked in neutral 3.5% NaCl solutions for long time (around 70 d) and Ni−P coating for around 7 d. With increasing immersion time, the OCP increases gradually from −0.36 to −0.28 V (vs SCE) for 120 h and then becomes more negative (around −0.5 V vs SCE) for 180 h, finally reaches around −0.41 V (vs SCE) after soaking for 800 h. During long-term immersion process, slight fluctuations appear in OCP within most immersion time and two obvious declines appear in the vicinity time of 200 and 700 h, and then return to more positive values. This suggests that Ni−P−TiN composite coatings have self-recovering function during long-term immersion in NaCl solution. Ni−P−TiN composite coatings can withstand Cl^- ion attack for more than 1600 h. The OCP of Ni−P coating immersed in 3.5% NaCl solution significantly decreases to more negative value (−1.35 V) at 170 h as shown in Fig. 9, which is different for Ni−P−TiN coating. AZ91D magnesium alloy with Ni−P−TiN composite coating is not attacked severely by Cl^- ion in NaCl solution and self-recovering

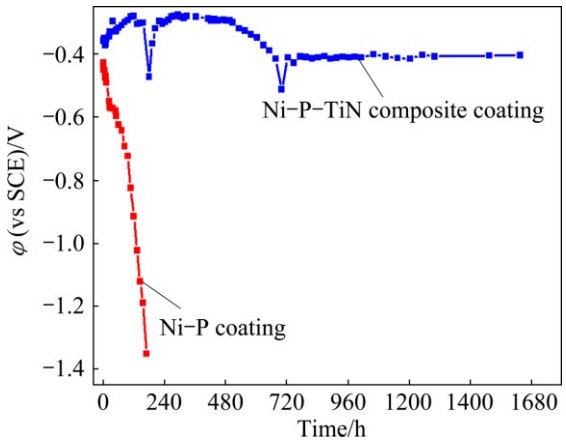

Fig. 9 OCP of Ni−P−TiN composite coating and Ni−P coating in neutral 3.5% NaCl solution at room temperature for different immersion time

since TiN nanoparticles are dispersed in Ni−P alloy plating [39].

From the Nyquist plot of Ni−P alloy coatings shown in Fig. 10, the impedance of Ni−P alloy coating is measured to be significantly higher than that of magnesium alloy, which is an indication of increasing the corrosion resistance of AZ91D magnesium alloy. Alternatively, it can be claimed that Ni−P alloy coating provides good anti-corrosive barrier for magnesium alloy.

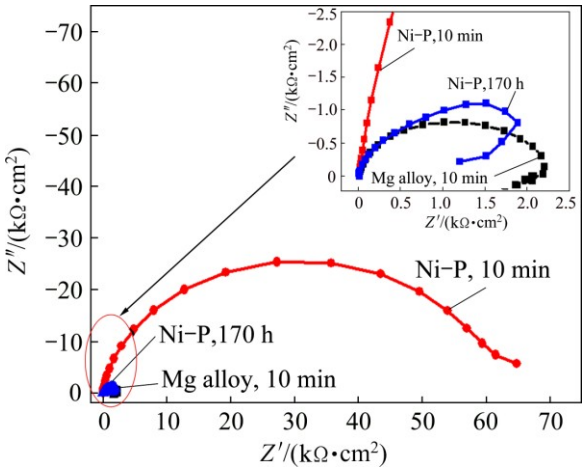

Fig. 10 Nyquist plots of AZ91D magnesium alloy substrate immersed for 10 min, AZ91D magnesium alloy coated with Ni−P alloys immersed for 10 min and 170 h, in neutral 3.5% NaCl solution at room temperature

The Nyquist plot of Ni−P coatings immersed in 3.5% NaCl solution for 170 h is very similar to that of uncoated AZ91D magnesium alloy, indicating that corrosion holes and cracks of Ni−P coating appear after 170 h immersion. EIS was also conducted to detect the corrosion resistance of Ni−P−TiN composite coatings. Figure 11 shows the Nyquist and Bode plots of Ni−P−TiN composite coatings after long-term immersion in neutral 3.5% NaCl solution under the OCP. The shape of Nyquist plots for Ni−P−TiN composite coatings in the measurement frequency range is flattening semi-elliptical with different diameter. It is well-known that the corrosion resistance of the coatings is determined by the diameter of semicircle, and the larger the diameter is, the better the corrosion resistance of the coatings is. The Bode plots for Ni−P−TiN composite coatings exhibit the broad peak (phase angle relative to the frequency) in the investigated frequency range of 10^5−10^{-2} Hz, which indicates that there are two time constants [12]. With extending the immersion time, the diameter of capacitive loop initially increases and then decreases afterwards indicating that the corrosion resistance of the Ni−P−TiN composite coating increases initially, and then decreases afterwards. Simultaneously, the shape of capacitive loop

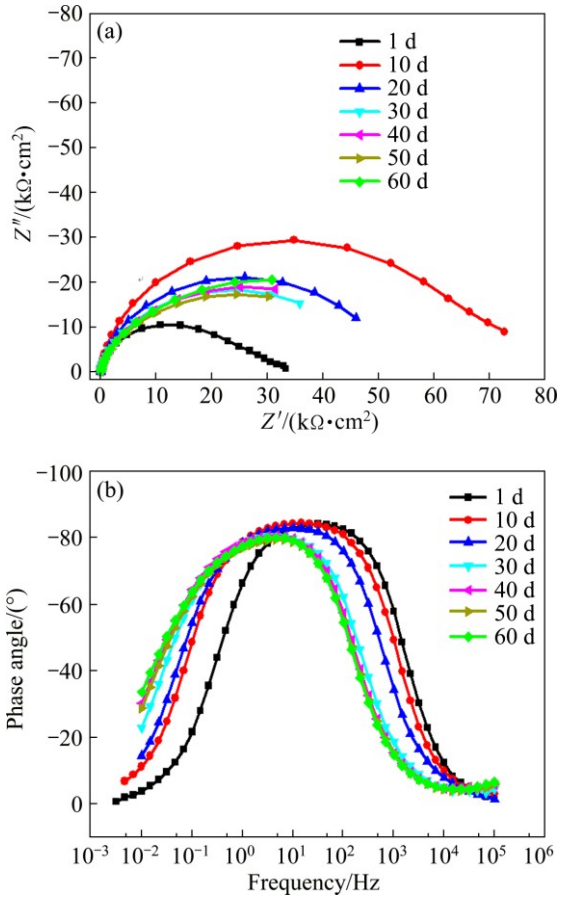

Fig. 11 Nyquist (a) and Bode (b) plots of Ni−P−TiN composite coating immersed in neutral 3.5% NaCl solution for long term at room temperature

is also changed from semi-elliptical shape into a quarter of the elliptical shape, which is reflected in Fig. 11(b). In the case of Ni−P−TiN composite coatings, the highest absolute value of phase angle decreases from 85° to 80° with increasing the immersion time. However, the frequency corresponding to the maximum phase angle gradually shifts to the lower value. The EIS data indicate that the corrosion behavior of composite coatings in corrosion solution changes and the capacitance characteristic of the coatings surface weakens [40]. It can be observed that the Ni−P−TiN composite coatings immersed in solution containing Cl^- for 1440 h can withstand corrosion without changing the impedance value of the composite coatings. Therefore, it can be claimed that the incorporation of TiN nanoparticles has dramatically affected the long-term corrosion resistance of Ni−P−TiN composite coatings.

In order to understand the corrosion resistance quantitatively, the equivalent circuit is used for fitting the EIS data of Ni−P−TiN composite coatings consisting of two time constants in series with constant phase element as shown in Fig. 12. It has been mentioned that the high frequency capacitive loop is related to the characteristics of the electric double layer formed by the metal surface and corrosion solution interface [41], which is described as R_{ct} and Q_{dl}. Q_f and R_f represent for coatings/metal interface capacitance and Ni/Ni−P−TiN film resistance, respectively. The fitted parameters are given in Table 4.

It is evident that R_s (electrolyte resistance) of Ni−P−TiN composite coating increases gradually with increasing the immersion time from 1 to 60 d. During 60 d immersion, R_{ct} of Ti−P−TiN coating increases from 19.66 to 45.01 kΩ·cm^2 in the first 10 d immersion and then decreases to 11.48 kΩ·cm^2 for the 60 d immersion. However, R_f follows the trend of R_{ct}, i.e., R_f increases

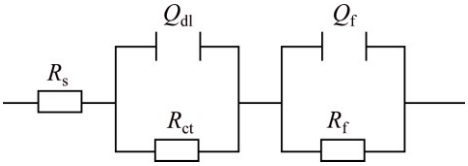

Fig. 12 Equivalent circuit model for observing corrosion behavior of Ni−P−TiN composite coatings immersed in neutral 3.5% NaCl solution for long-term at room temperature

Table 4 Best fitting values of equivalent circuit elements shown in Fig. 12

Sample	Immersion time	R_s/(Ω·cm^2)	R_{ct}/(kΩ·cm^2)	Q_{dl}/(μF·cm^{-2})	n_{dl}	R_f/(kΩ·cm^2)	Q_f/(μF·cm^{-2})	n_f	(R_f+R_{ct})/(kΩ·cm^2)
AZ91D Mg alloy	10 min	6.53	1.06	24.20	1	1.13	7.37	0.92	2.19
Ni−P	10 min	7.56	14.22	24.64	0.94	46.82	23.72	0.94	61.04
	170 h	6.48	0.80	31.12	1	2.06	96.56	1	2.86
Ni−P−TiN	1 d	5.79	19.66	24.39	0.96	11.72	0.03	0.84	31.38
	10 d	6.14	45.01	0.35	0.96	27.67	1.89	0.91	72.68
	20 d	6.59	29.45	1.63	0.99	19.98	0.77	0.91	49.43
	30 d	9.61	16.05	1.39	0.89	28.99	0.03	0.99	45.04
	40 d	9.68	11.71	1.95	0.88	34.07	0.04	0.99	45.78
	50 d	10.69	11.33	1.88	0.87	30.16	0.04	0.99	41.49
	60 d	11.17	11.48	1.92	0.88	36.75	0.04	0.99	48.23

from 31.38 to 72.68 kΩ·cm^2 and then reduces to 45.00 kΩ·cm^2. R_{ct} values of uncoated AZ91D magnesium alloy and Ni−P coating are found to be 1.06 and 14.22 kΩ·cm^2 for first 10 min immersion, respectively. On the other hand, R_{ct} for Ni−P coating dramatically decreases to 0.80 kΩ·cm^2 for 170 h immersion, which is even lower than that of the uncoated AZ91D magnesium alloy.

When Ni−P−TiN composite coatings are immersed in 3.5% NaCl solution, Cl^- tends to be adsorbed on some special sites of the coating surface, such as lattice defects point or high Ni content area [25]. As a result, corrosion product, $NiCl_2$, is formed on the surface of Ni−P−TiN composite coatings. During the initial stage, phosphorus is continuously accumulated on the composite coating surface resulting in the coatings with high phosphorus content. The coating surface with high phosphorus shows passivation and better corrosion resistance [5]. With the extension of immersion time, Ni dissolves continuously and makes pit. However, the existence of TiN nanoparticles in the composite coating inhibits the corrosion process, which shows steady corrosion resistance in the Ni−P−TiN composite coatings for a long time.

From the aforementioned data, it can be assumed that the corrosion process of Ni−P−TiN composite coatings includes three stages. First of all, the impedance value increases during early stage of immersion (10 d). Then, the relatively stable impedance value with little fluctuation appears in the middle stage of immersion (20 to 50 d). Eventually, localized pitting corrosion presents in the third stage. If corrosive medium reaches to the interface of composite coatings and substrate, serious galvanic corrosion will also occur. Thus, magnesium alloy substrate will be destroyed completely, even if only a corrosion point perforates on the composite coatings.

Compared with Ni−P alloy coatings shown in Fig. 4, the surface and microstructure of Ni−P−TiN composite coating appear to be smoother and more compact, respectively. The amount of micro-cracks in coatings reduces significantly resulting in higher density of composite plating. Therefore, aggressive ions, such as Cl^-, could not penetrate into the substrate through the surface of composite coating, and the superior corrosion resistance of composite coating is found. During the immersion process of Ni−P−TiN composite, TiN nanoparticles can accumulate in the micro-cracks of the composite coatings surface and blocks the corrosion channel for corrosive medium to enter into the interior of composite coatings. This reduces the corrosion rate of magnesium alloy by Ni−P−TiN composite coating. In addition, as the chemical stability of TiN nanoparticle is very good, high corrosion resistance properties in acid, alkali and salt medium are expected. Therefore, it can be concluded that TiN nanoparticles distributed uniformly into the surface of the composite coating can prevent the growing of localized corrosion, even the formation of corrosion pits and holes. Thus, improvement in the corrosion resistance is expected for composite coatings.

4 Conclusions

1) The Ni−P coatings with/without TiN nano-particles show much higher hardness than that of uncoated magnesium alloy. Ni−P−TiN composite coating improves the hardness of the substrate to a greater extent than that of Ni−P coating. Subsequent heat treatment at 400 °C for 1 h further improves the Vickers hardnesses of Ni−P and Ni−P−TiN composite coatings.

2) Compared with Ni−P−TiN composite coating, Ni−P alloy coating shows better corrosion resistance for short-term immersion. However, TiN nanoparticles in composite coating play a significant role for long-term corrosion resistance. For example, Ni−P−TiN composite coating immersed in NaCl solution for 1600 h can withstand corrosion, while the corrosion resistance of Ni−P alloy coating shows a dramatic decrease after 180 h immersion. There is a significant self-recovering process of Ni−P coating containing TiN nanoparticles, which is beneficial to improving the corrosion resistance of AZ91D magnesium alloy for long period immersion.

References

[1] TANG J W, AZUMI K. Effect of copper pretreatment on the zincate process and subsequent electroplating of a protective copper/nickel deposit on the AZ91D magnesium alloy [J]. Electrochimica Acta, 2011, 56(24): 8776−8782.

[2] GRAY J E, LUAN B. Protective coatings on magnesium and its alloys—A critical review [J]. Journal of Alloys and Compounds, 2001, 336(1−2): 88−113.

[3] ALVAREZ R B, MARTIN H J, HORSTEMEYER M F, CHANDLER M Q, WILLIAMS N, WANG P T, RUIZ A. Corrosion relationships as a function of time and surface roughness on a structural AE44 magnesium alloy [J]. Corrosion Science, 2010, 52(5): 1635−1648.

[4] BENDER S, GOELLNER J, ATRENS A. Corrosion of AZ91 in 1N NaCl and the mechanism of magnesium corrosion [J]. Advanced Engineering Materials, 2008, 10(6): 583−587.

[5] MAHALLAWY N E, BAKKAR A, SHOEIB M, PALKOWSKI H, NEUBERT V. Electroless Ni−P coating of different magnesium alloys [J]. Surface and Coatings Technology, 2008, 202(21): 5151−5157.

[6] CHEN X B, YANG H Y, ABBOTT T B, EASTON M A, BIRBILIS N. Corrosion-resistant electrochemical platings on magnesium alloys: A State-of-the-art review [J]. Journal of Science and Engineering, 2012, 68(6): 518−535.

[7] SUN Can, GUO Xing-wu, WANG Shao-hua, GUO Jia-cheng, DING Wen-jiang. Homogenization pretreatment and electroless Ni−P plating on AZ91D magensium alloy [J]. Transaction of Nonferrous Metals Society of China, 2014, 24(12): 3825−3833.

[8] LEE J, CHUNG W, JUNG U, KIM Y. Direct nickel electrodeposition on magnesium alloy in pyrophosphate electrolyte [J]. Surface and Coatings Technology, 2011, 205(16): 4018−4023.

[9] HUANG C A, WANG T H, WEIRICH T, NEUBERT V. Electrodeposition of a protective copper/nickel deposit on the magnesium alloy (AZ31) [J]. Corrosion Science, 2008, 50(5): 1385−1390.

[10] CHEN W W, GAO W, HE Y D. A novel electroless plating of Ni−P−TiO_2 nano-composite coatings [J]. Surface and Coatings Technology, 2010, 204(15): 2493−2498.

[11] ZOIKIS-KARATHANASIS A, PAVLATOU E A, SPYRELLIS N. Pulse electrodeposition of Ni−P matrix composite coatings reinforced by SiC particles [J]. Journal of Alloys and Compounds, 2010, 494(1−2): 396−403.

[12] BALARAJU J N, EZHIL SELVI V, RAJAM K S. Electrochemical behavior of low phosphorus electroless Ni−P−Si_3N_4 composite coatings [J]. Materials Chemistry and Physics, 2010, 120(2−3): 546−551.

[13] SUZUKI Y, ARAI S, ENDO M. Ni−P alloy-carbon black composite films fabricated by electrodeposition [J]. Applied Surface Science, 2010, 256(22): 6914−6917.

[14] SHEU H H, HUANG P C, TSAI L C, HOU K H. Effects of plating parameters on the Ni−P−Al_2O_3 composite coatings prepared by pulse and direct current plating [J]. Surface and Coatings Technology, 2013, 235: 529−535.

[15] YANG Y J, CHEN W W, ZHOU C G, XU H B, GAO W. Fabrication and characterization of electroless Ni−P−ZrO_2 nano-composite coatings [J]. Applied Nanoscience, 2011, 1(1): 19−26.

[16] LIU Y Y, YU J, HUANG H, XU B H, LIU X L, GAO Y, DONG X L. Synthesis and tribological behavior of electroless Ni−P−WC nanocomposite coatings [J]. Surface and Coatings Technology, 2007, 201(16-17): 7246−7251.

[17] XIA F F, LIU C, WANG F, WU M H, WANG J D, FU H L, WANG J X. Preparation and characterization of nano Ni−TiN coatings deposited by ultrasonic electrodeposition [J]. Journal of Alloys and Compounds, 2010, 490(1−2): 431−435.

[18] MAFI I R, DEHGHANIAN C. Studying the effects of the addition of TiN nanoparticles to Ni−P electroless coatings [J]. Applied Surface Science, 2011, 258(5): 1876−1880.

[19] MATHIEU C R S, HAZAN J, STEINMETZ P. Corrosion behaviour of high pressure die-cast and semi-solid cast AZ91D alloys [J]. Corrosion Science, 2002, 44(12): 2737−2756.

[20] BRUNELLI K, DABALÀ M, CALLIARI I, MAGRINI M. Effect of HCl pre-treatment on corrosion resistance of cerium-based conversion coatings on magnesium and magnesium alloys [J]. Corrosion Science, 2005, 47(4): 989−1000.

[21] YU L H, HUANG W G, ZHAO X. Preparation and characterization of Ni−P–nanoTiN electroless composite coatings [J]. Journal of Alloys and Compounds, 2011, 509(10): 4154−4159.

[22] TANG J Q, AZUMI K. Influence of zincate pretreatment on adhesion strength of a copper electroplating layer on AZ91D magnesium alloy [J]. Surface and Coatings Technology, 2011, 205(8−9): 3050−3057.

[23] WANG Xin-juan, YU Gang, OUYANG Yue-jun, HE Xiao-mei, ZHANG Jun, YE Li-yuan. One-step pickling-activation before magnesium alloy plating [J]. Transactions of Nonferrous Metals Society of China, 2009, 19(2): 504−510.

[24] ZHAO M J, CAI C, WANG L, ZHANG Z, ZHANG J Q. Effect of zinc immersion pretreatment on the electro-deposition of Ni onto AZ91D magnesium alloy [J]. Surface and Coatings Technology, 2010, 205(7): 2160−2166.

[25] ZHANG S, CAO F H, CHANG L R, ZHENG J J, ZHANG Z, ZHANG J Q, CAO C N. Electrodeposition of high corrosion resistance Cu/Ni−P coating on AZ91D magnesium alloy [J]. Applied Surface Science, 2011, 257(21): 9213−9220.

[26] ZHU Xu-bei, CAI Chao, ZHENG Guo-qu, ZHANG Zhao, LI Jin-feng. Electrodeposition and corrosion behavior of nanostructured Ni−TiN composite films [J]. Transactions of Nonferrous Metals Society of China, 2011, 21(10): 2216−2224.

[27] XIE Z H, YU G, HU B N, LEI X P, LI T J, ZHANG J. Effects of $(NH_4)_2SO_4$ on the characteristics of the deposits and properties of an electroless Ni−P plating solution [J]. Applied Surface Science, 2011, 257(11): 5025−5031.

[28] ZHAO M C, LIU M, SONG G , ATRENS A. Influence of pH and chloride ion concentration on the corrosion of Mg alloy ZE41 [J]. Corrosion Science, 2008, 50(11): 3168−3178.

[29] ALLAHKARAM S R, NAZARI M H, MAMAGHANI S, ZAREBIDAKI A. Characterization and corrosion behavior of electroless Ni−P/nano-SiC coating inside the CO_2 containing media in the presence of acetic acid [J]. Materials & Design, 2011, 32(2): 750−755.

[30] CAI C, ZHU X B, ZHENG G Q, YUAN Y N, HUANG X Q, CAO F H, YANG J F, ZHANG Z. Electrodeposition and characterization of nano-structured Ni−SiC composite films [J]. Surface and Coatings Technology, 2011, 205(11): 3448−3454.

[31] MA C B, CAO F H, ZHANG Z, ZHANG J Q. Electrodeposition of amorphous Ni−P coatings onto Nd-Fe-B permanent magnet substrates [J]. Applied Surface Science, 2006, 253(4): 2251−2256.

[32] PISCANEC S, CIACCHI L C, VESSELLI E, COMELLI G, SBAIZERO O, MERIANI S, VITA A D. Bioactivity of TiN-coated titanium implants [J]. Acta Materialia, 2004, 52: 1237−1245.

[33] NATTER H, HEMPELMANN R. Tailor-made nanomaterials designed by electrochemical methods [J]. Electrochimica Acta, 2003, 49(1): 51−61.

[34] GOU Yin-ning, HUANG Wei-jiu, ZENG Rong-chang, ZHU Yi. Influence of pH values on electroless Ni−P−SiC plating on AZ91D magnesium alloy [J]. Transactions of Nonferrous Metals Society of China, 2010, 20(S): s674−s678.

[35] ORDINE A P, DÍAZ S L, MARGARIT I C P, BARCIA O E, MATTOS O R. Electrochemical study on Ni−P electrodeposition [J]. Electrochimica Acta, 2006, 51(8−9): 1480−1486.

[36] RANGANATHA S, VENKATESHA T V, VATHSALA K. Development of electroless Ni−Zn−P/nano-TiO_2 composite coatings and their properties [J]. Applied Surface Science, 2010, 256(24): 7377−7383.

[37] HUANG Y S, ZENG X T, ANNERGREN I, LIU F M. Development of electroless NiP−PTFE−SiC composite coating [J]. Surface and Coatings Technology, 2003, 167(2−3): 207−211.

[38] WANG Ping, CHENG Ying-liang, ZHANG Zhao. A study on the electrocodeposition processes and properties of Ni−SiC nanocomposite coatings [J]. Journal of Coatings Technology and Research, 2010, 8(3): 409−417.

[39] MALFATTI C F, ZOPPAS FERREIRA J, SANTOS C B, SOUZA B V, FALLAVENA E P , VAILLANT S, BONINO J P. NiP/SiC composite coatings: The effects of particles on the electrochemical behaviour [J]. Corrosion Science, 2005, 47(3): 567−580.

[40] BALARAJU J, SANKARA N, SESHADRI S. Evaluation of the corrosion resistance of electroless Ni−P and Ni−P composite coatings by electrochemical impedance spectroscopy [J]. Journal of Solid State Electrochemistry, 2001, 5(5): 334−338.

[41] WANG L L, CHEN H J, HAO L, LIN A, GAN F X. Electrochemical corrosion behavior of electroless Ni−P coating in NaCl and H_2SO_4 solutions [J]. Materials and Corrosion, 2010, 62(11): 1003−1007.

AZ91D 镁合金 Ni−P−TiN 复合涂层的电沉积制备及其耐蚀性能

周亚茹[1]，张 珊[1]，聂林林[1]，朱泽洁[1]，张鉴清[1]，曹发和[1]，张俊喜[2]

1. 浙江大学 化学系，杭州 310027；
2. 上海电力学院 上海市电力材料防护与新材料重点实验室，上海 200090

摘 要：为了提高 AZ91D 镁合金的耐蚀性能和显微硬度，通过电沉积方法制备 TiN 纳米粒子掺杂的 Ni−P−TiN 复合涂层。应用扫描电镜、能谱和 XRD 等手段研究涂层的表面、界面形貌和显微组成，并结合电化学方法研究涂层的耐蚀性能。研究结果表明，经过活化、浸锌和预镀层等系列复杂前处理，可有效提高镁合金在电镀液中的稳定性和涂层结合力，TiN 纳米粒子可以通过电沉积方式掺杂至 Ni−P 基体中。TiN 纳米颗粒和后续热处理可以有效提高 Ni−P 涂层的显微硬度。腐蚀结果表明 Ni−P−TiN 复合涂层的耐蚀性能比裸 AZ91D 镁合金大幅增加。在短期浸泡内，Ni−P−TiN 的耐蚀性能与没有 TiN 纳米粒子掺杂的 Ni−P 涂层相当，但 TiN 纳米粒子对于提高复合涂层长期耐蚀性能具有重要影响。

关键词：AZ91D；复合涂层；TiN 纳米粒子；电沉积；耐蚀性能

(Edited by Xiang-qun LI)